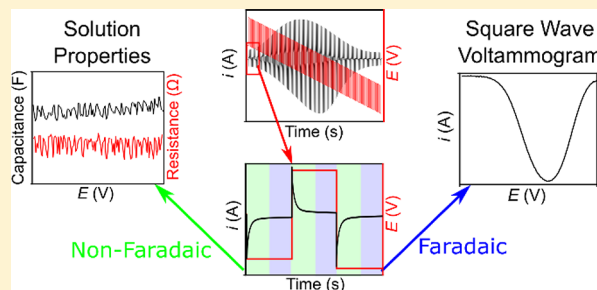


Enhancing Square Wave Voltammetry Measurements via Electrochemical Analysis of the Non-Faradaic Potential Window

Samuel J. Cobb^{†,‡} and Julie V. Macpherson^{*,†}[†]Department of Chemistry, University of Warwick, Coventry CV4 7AL, U.K.[‡]Diamond Science and Technology CDT, University of Warwick, Coventry CV4 7AL, U.K.

Supporting Information

ABSTRACT: Square wave voltammetry (SWV) is most commonly used to enhance electroanalytical current signals of a redox analyte of interest. The SWV is typically recorded in a potential region where both non-faradaic and faradaic currents are collected; however, only data in the faradaic region are analyzed. In this article, we show how by collecting the full current–time (i – t) data, arising from the SWV potential pulse sequence, and analyzing in the region of the potential scan where non-faradaic currents arise, further analytical information can be collected, over short time periods (typically seconds). Importantly, we show how information on solution resistance, R (and solution conductivity), and double layer capacitance, C , can be extracted from this data, without the need to conduct further electrochemical experiments, such as electrochemical impedance spectroscopy or independent solution conductivity measurements. Knowledge of the latter is important for measurements in real world samples, where the electrolyte concentration is unknown. We show how SWV measurements of electrode capacitance with repeat SWV scans can also be used to determine whether a changing faradaic SWV signal is due to electrode fouling or changing analyte concentration. Finally, knowledge of both parameters (RC) is essential for optimization of the SWV parameters, such that the faradaic SWV signal is truly free from non-faradaic contributions.



In electroanalysis, pulsed voltammetric techniques are a common way of increasing detection sensitivity,¹ with the aim of excluding capacitive contributions from the response and lowering detection limits. Square wave voltammetry (SWV), originally developed by Kalousek and Barker,² is particularly popular,³ as it allows faster analysis times compared to other pulse techniques, such as differential pulse voltammetry or normal pulse voltammetry.¹ For most analytical applications, staircase SWV, proposed by Ramaley and Krause,^{4,5} but often referred to as SWV (or Osteryoung SWV),⁶ has become the de facto standard. SWV is widely used in electroanalytical studies, interestingly, often with little or no comment as to how the operational parameters are chosen.

SWV involves the application of a series of potential pulses, formed from a potential staircase (Figure 1a, dashed line) overlaid with a square wave pulse, with a forward and then reverse pulse occurring on each tread of the staircase (Figure 1a, solid line).³ Operational variables include the pulse amplitude, (E_{SW}) frequency (f_{SW}) and staircase increment (E_1), creating a large parameter space for SWV optimization. The raw data consists of a series of current time (i – t) decays in the anodic and cathodic directions, where the length of the decay is determined by the frequency employed.

An example i – t curve in a single square wave pulse (blue line), for detection of a redox active analyte, is shown in Figure 1b, where the current passed represents the sum of the faradaic (I_F , red line, diffusional $t^{-1/2}$ decay⁷) and non-faradaic (I_{NF} ,

black line, exponential t decay) current. With the text book definition of SWV, the current at the end of each pulse is sampled, and the reverse current is subtracted from the forward current and plotted against the staircase potential to give a voltammogram. However, to improve on noise, most commercial potentiostats current average over a defined percentage of the pulse (as much as 50–100% of each individual i – t trace).⁸ Some potentiostats also record the forward and reverse currents in the output data for inspection by the user.

In a potential range where no faradaic reactions occur, the electrode can be treated as ideally polarizable, and the shape of the i – t decay curve relates to uncompensated resistance, R , and capacitance, C , which collectively represent the time constant, RC , as shown by eq 1, where ΔE represents the potential pulse height (which is $2E_{SW} + E_1$ for the forward pulse and $2E_{SW}$ for the reverse pulse).

$$i(t) = \frac{\Delta E}{R} e^{-t/RC} \quad (1)$$

The uncompensated resistance is related to the cell geometry and electrode spacing, electrode resistance, and solution resistance.⁹ If the cell geometry is fixed and the

Received: April 16, 2019

Accepted: May 14, 2019

Published: May 14, 2019

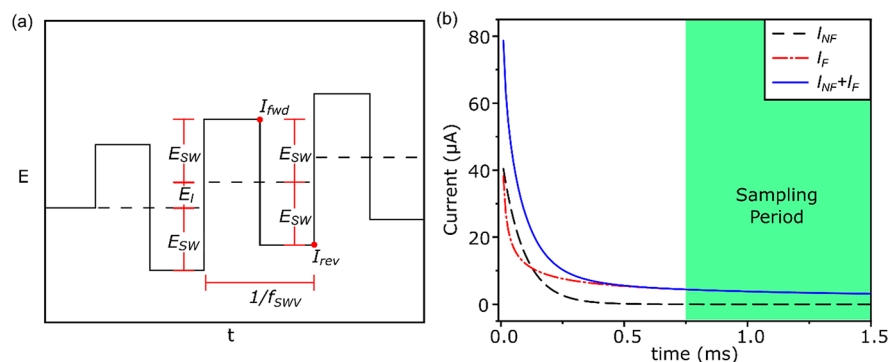


Figure 1. (a) SWV potential pulse sequence, where E_{SW} is the amplitude, f_{SW} is the square wave frequency, E_I is the increment, and I_{fwd} and I_{rev} are the end of pulse sampling points for the forward and reverse currents, respectively. (b) Theoretical I_{NF} , I_F , and $(I_{NF} + I_F)$ i - t responses for an anodic potential pulse of $\Delta E = 0.1$ V, $R = 3$ k Ω , $C_{dl} = 40$ nF, diffusion coefficient = 8×10^{-6} cm 2 s $^{-1}$, and concentration = 0.1 mM.

electrode resistance negligible, the uncompensated resistance depends only on solution resistance. In theory the conditions of SWV should be chosen such that sampling occurs at a time (or time period) in the i - t curve where the non-faradaic currents have decayed to ~ 0 , and only the faradaic response is analyzed. In systems where R and/or C are high, low frequencies and small amplitudes should be used for sensitive faradaic analysis; however, this is at the expense of long measurement times and reduced faradaic currents. In the presence of faradaic electron transfer (ET), kinetic and mechanistic information on ET processes is also possible, for example from analyzing the relationship between peak current and frequency,^{10–12} or amplitude.^{13–16}

In SWV, focus is always on the faradaic ET reaction. However, by sampling in a potential region of the SWV where only non-faradaic (double layer charging) reactions are captured, using appropriate sampling conditions, extraction of information on R and C should be possible. R can be used to inform on solution conductivity (σ) and C on the double layer capacitance (C_{dl}) of the electrode. Information on the former is important for a large number of applications, including drinking water quality assessment, process water monitoring, production of ultrapure water, and measurement of the salinity of seawater.¹⁷ In contrast, C can be used to inform on changes that are taking place at the electrode surface, as a function of time, e.g., electrode fouling,^{18–20} common in more complex real world solution matrices. Knowledge of RC can also be used to provide feedback on the most appropriate parameters for faradaic SWV analysis. Note, electrochemical impedance spectroscopy (EIS) is typically used as the method of choice for determining R and C , along with providing information on ET kinetics.²¹ However, EIS measurements can be time-consuming and require additional hardware. AC voltammetry techniques have similarities to pulsed DC techniques, such as SWV,²² with it being possible to form a square wave pulse from a combination of sine waves.²³ Through Fourier transformation and modeling of this response, it is possible to extract information on R and C , in addition to information on the faradaic process;²³ however, the analysis of data is not as immediately intuitive and requires simulation.²⁴

In this article, we show how by analyzing the SWV response in the non-faradaic region typically just prior to the on-set of the faradaic reaction and by using the part of the i - t trace that is often discarded in conventional SWV, it is possible to provide additional information on (i) optimization data for subsequent faradaic SWV analysis (ii) solution conductivity

and (iii) surface modification/fouling processes taking place during subsequent scans. For these proof-of-concept studies, we employ boron-doped diamond (BDD) electrodes, given BDD offers a wider potential range over which non-faradaic processes occur.²⁵

EXPERIMENTAL SECTION

Solutions. All solutions were prepared from ultrapure water (Milli-Q, Millipore Corp.) with a resistivity of 18.2 M Ω cm at 25 °C. Potassium nitrate (KNO $_3$, 99.97%; Sigma-Aldrich) and potassium chloride (KCl, $\geq 99\%$; Sigma-Aldrich) were used as supporting electrolytes at different concentrations to adjust σ . The σ and resistivity (ρ) of all solutions was measured independently using a commercial four-point graphite probe conductivity sensor (InLab 731, Mettler Toledo; range 10^1 – 10^6 μ S cm $^{-1}$, nominal cell constant (κ) of 0.57 cm $^{-1}$). 0.5% w/v mucin from porcine stomach ($\geq 99\%$; Sigma-Aldrich) and serotonin hydrochloride ($\geq 98\%$; Sigma-Aldrich) were used for fouling experiments with σ adjusted using KCl. Hexaamineruthenium(III)chloride (Ru(NH $_3$) $_6$ Cl $_3$, $> 97\%$, Strem Chemicals) was used for electrode characterization. Water samples were collected from Bassenthwaite, Lake District, UK; Hayle estuary, Cornwall, UK; Kenilworth river, Warwickshire, UK; and laboratory taps at the University of Warwick, UK. For the laser micromachined BDD electrode, pH 7.09, Carmody buffer was prepared using boric acid (H $_3$ BO $_3$, 99.97%; Sigma-Aldrich), citric acid (C $_6$ H $_8$ O $_7$, $\geq 99.5\%$; Sigma-Aldrich), and tertiary sodium phosphate (Na $_3$ PO $_4$, $\geq 95\%$; Sigma-Aldrich) with a buffer capacity of 25–30 mM per pH unit.²⁶

Electrochemical Set-up. For electrochemical measurements, a three-electrode configuration was utilized. An 1 mm diameter BDD disk, doped above the metallic threshold (minimal sp 2 content) and encapsulated with insulating diamond, was used as the working electrode (WE). Fabrication of this electrode is described elsewhere.²⁷ For sp 2 carbon-incorporated-BDD electrode experiments, a glass-sealed 1 mm BDD disk electrode containing a laser micromachined hexagonal array of 61, 50 μ m diameter sp 2 -containing pits, with a center-to-center spacing of 100 μ m, was employed.^{28,29} A platinum wire was used as the counter electrode (CE) and a saturated calomel electrode (SCE) as the reference electrode (RE). The electrode spacing and geometry were controlled, with the RE and WE in the same plane, at an electrode center-to-center distance of 5 mm. All measurements were performed using an Ivium compactstat (Ivium Technologies B.V.).

A series of potential pulses were applied, and the resulting $i-t$ traces were recorded. E_{SW} , f_{SW} , and E_I were chosen to simulate an SWV measurement, as illustrated by the data in S11. For all studies, the potentiostat filter was set to 1 MHz, and the high speed mode was used for stability to avoid additional processing of the data by the instrument. For $f_{SW} \leq 25$ Hz, the sampling frequency (f_{smp}) was 1 kHz, limited by the data transfer rate. At $f_{SW} > 25$ Hz, f_{smp} was $60 \times f_{SW}$, limited by the onboard potentiostat memory to 8192 data points for the entire scan. Complementary EIS studies were conducted at a potential at the midpoint of the corresponding SWV and in a region free from faradaic currents, with an amplitude of 10 mV at 16 equally spaced frequencies from 10 Hz to 1 MHz.

Data Analysis. All data were analyzed using Matlab R2018a (Mathworks). Each potential pulse was extracted and fitted with exponential decays using the curve fitting toolbox.

RESULTS AND DISCUSSION

Extracting σ and C Data from a SWV Signal. The insert to Figure 2 shows the cyclic voltammetric (CV) response for a

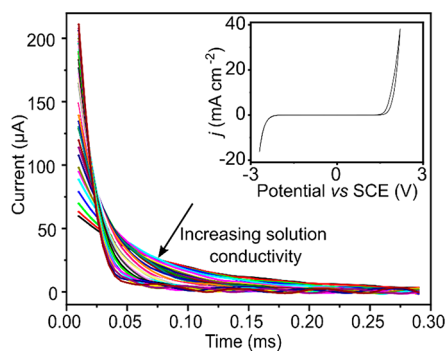


Figure 2. $i-t$ decays ($n = 35$) for a single cathodic potential pulse taken in the region where only non-faradaic reactions occur (0 to 0.2 V vs SCE) in solutions from 2 to 24 mS cm^{-1} . (Inset) CV recorded at 0.1 V s^{-1} in 0.1 M KCl, for BDD.

BDD electrode in a 0.1 M KCl electrolyte (scan rate = 0.1 V s^{-1}). The CV is almost featureless as a result of inner sphere redox processes, such as water electrolysis and the oxygen reduction reaction, being kinetically hindered.^{25,30} The cathodic window is dominated by the hydrogen evolution reaction³¹ and the anodic by chloride oxidation.³² There is a

large potential window (~ -1.3 to $+1.0$ V vs SCE) in which the current response is dominated by double layer capacitance. In this potential range, the raw $i-t$ data from a SWV will depend only on R and C . Figure 2 shows representative $i-t$ data, taken from a single potential step in the SWV (0.0–0.2 V vs SCE over a time period of 0.3 ms, i.e., $f_{SW} = 1.67 \text{ kHz}$) for $n = 35$ solutions of different electrolyte concentrations (i.e., σ) across the range of 2 (0.022 M KCl)–24 mS cm^{-1} (0.25 M KCl).

As σ decreases, the decay time length increases, which is in accordance with eq 1. The time at which the data is free from RC contributions is assumed to be where the non-faradaic current is less than the resolution of the potentiostat 16-bit analogue to digital converter for a $100 \mu\text{A}$ current range (3 nA). At the highest σ , 24 mS cm^{-1} (0.25 M KCl), current sampling at times ≥ 0.12 ms ($f_{SW} \leq 416$ Hz) are recommended, and at the lowest σ used in this study, 20 $\mu\text{S cm}^{-1}$ (0.002 M KCl) times of ≥ 82 ms ($f_{SW} \leq 6$ Hz) are required. These times set limits on the SWV sampling frequency for truly RC free contributions to the current.

In SWV, many pulses are recorded, with the exact number being controlled by E_I and the potential scan range of interest. Both the forward and reverse $i-t$ curves, per potential step, can be analyzed using eq 1. The modulus of the current response in each pulse can be analyzed using an exponential fit of the form

$$|i| = A \times \exp(B \times t) \quad (2)$$

where, in accordance with eq 1, the pre-exponential term A represents $(\Delta E/R)$, where ΔE for a forward pulse is larger than the reverse pulse by the increment, and B is $(-1/RC)$. From A as ΔE is known, R can be experimentally determined for each pulse, as shown in Figure 3a, for a solution containing 0.25 M KCl ($\sigma = 24 \text{ mS cm}^{-1}$). Here, 246 potential pulses were applied in the cathodic direction over the non-faradaic potential range, +0.3 to -0.2 V vs SCE, with $E_{SW} = 0.1$ V and $E_I = 4$ mV. E_{SW} was chosen to give measurable current decays while E_I gave a reasonable (~ 0.5 V) potential scan range.

The data in Figure 3 is exemplar of the response across the σ range investigated and was chosen as one of the highest σ studied, with the fast RC decay making it one of the most challenging solution conditions for this measurement. The black and red data sets correspond to forward and reverse pulses, respectively. Figure 3a shows that neither the direction of ΔE nor the absolute potential applied affect the measured R values. The extracted R values are within the measurement

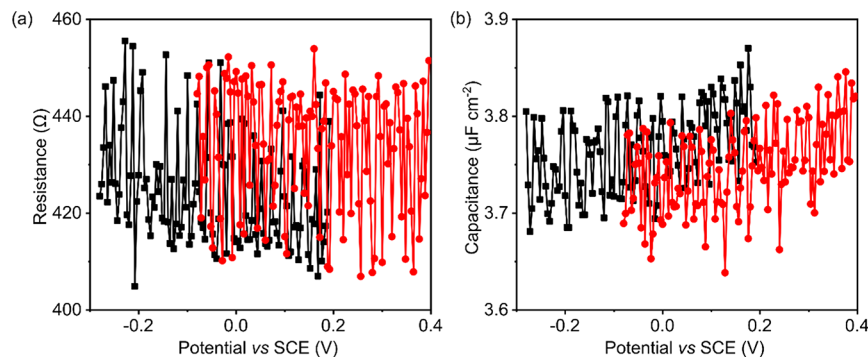


Figure 3. Effect of electrode potential on (a) the fitted R values and (b) C values for the forward (black) and reverse (red) pulses in a solution of 0.25 M KCl. $E_{SW} = 0.1$ V and $E_I = 4$ mV.

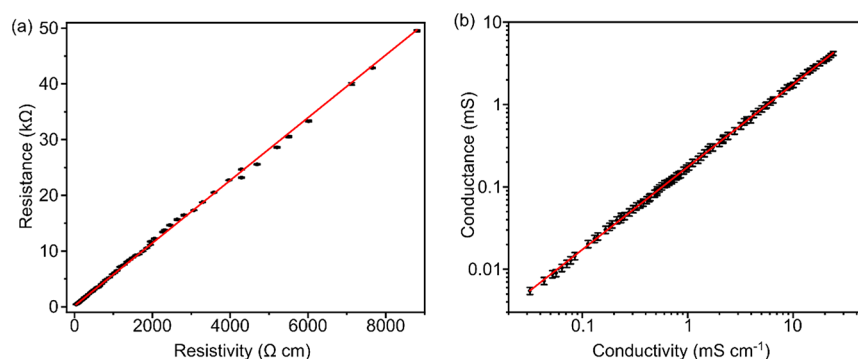


Figure 4. (a) Average measured R values in KCl ($n = 246$ for each R , error bars are standard deviation) in solutions of known ρ from SWV, with the y -intercept of which represents the additional system R that, when excluded, gives R_{sol} . (b) Average measured solution G in KCl ($n = 246$ for each G , error bars are standard deviation) from SWV in solutions of differing σ (gradient = 0.176 ± 0.002 , $R^2 = 0.999$).

uncertainty across the entire potential range scanned, independent of pulse direction. Thus, it is possible to use the mean value for the R values obtained from all the pulses to give a single value, $R = 429 \pm 13 \Omega$ ($n = 246$, mean \pm standard deviation). The large amount of data collected in one SWV scan provides accurate mean values for R on a short time scale; here, 246 individual measurements are captured in less than a second.

With knowledge of R , it is now possible to determine C for each pulse from the exponential term B in eq 2, as shown in Figure 3b. Unlike R , C and, in particular, C_{dl} of the electrode can have a dependence on the absolute potential and current direction.³³ However, BDD in aqueous solutions over the comparatively small potential range employed (0.3 to -0.2 V vs SCE) has been shown to have an almost flat capacitance–potential relationship,^{34–36} which is in agreement with our data. As such, C is averaged to give a value for the entire scan, in this case, $3.76 \pm 0.04 \mu\text{F cm}^{-2}$ ($n = 246$, mean \pm standard deviation). A complementary EIS measurement for the same 0.25 M KCl solution at 0.1 V vs SCE gave a value for C , in very close agreement, $= 3.80 \pm 0.11 \mu\text{F cm}^{-2}$, when fitted with a simple RC circuit (a resistor and capacitor in series). C_{dl} can have a concentration³⁷ and electrolyte dependence,³⁸ as the thickness of the Stern layer and ion mobility changes. The C measurements across the σ range of $20 \mu\text{S cm}^{-1}$ – 24 mS cm^{-1} at the BDD electrode are shown in SI2, with no specific trend observed, and an average value of $3.71 \pm 0.23 \mu\text{F cm}^{-2}$ ($n = 45\,510$, 185 measurements in solutions of differing conductivities, each of 246 pulses) calculated. These values agree well with previously published values for very similarly grown and prepared BDD, using CV measurements alone over the potential range of ± 0.1 V vs SCE; $C = 2.7$ – $7.7 \mu\text{F cm}^{-2}$.^{27,39}

Measurement of σ Using SWV. To assess whether i – t traces from the non-faradaic potential region of an SWV could be used to quantify σ , initial experiments considered the KCl electrolyte system over the σ range of $20 \mu\text{S cm}^{-1}$ (0.002 M KCl)– 24 mS cm^{-1} (0.25 M KCl), covering the typical σ range of river (~ 0.05 – 1.5 mS cm^{-1}), tap (~ 0.05 – 0.5 mS cm^{-1}), and industrial wastewater ($\sim 10 \text{ mS cm}^{-1}$), as well as typical supporting electrolyte concentrations used in electroanalytical measurements. SWV was employed using the conditions *vide supra*. As σ increases, and the RC time constant decreases, faster sampling is required to accurately capture the RC decay and vice versa. The onboard memory of the potentiostat employed limits the number of possible data points; therefore,

f_{samp} and f_{SW} must be changed throughout the conductivity range to accurately capture the RC decay.

The R values from the RC decay are the uncompensated R , which represents several series R s between the WE and RE. At low σ , R is dominated by the solution R (R_{sol}), and at high σ , other, solution independent resistances in the system, e.g., the electrode and wire resistances, will become more significant. These must be accounted for in order for the measured R term to correctly reflect R_{sol} . Figure 4a shows a plot of average measured R values vs the measured solution resistivity ($\rho = 1/\sigma$, $n = 246$ per different solution ρ employed), with the latter measured using a commercial conductivity meter, for the range $42 \Omega \text{ cm}$ – $50 \text{ k}\Omega \text{ cm}$ ($\sigma = 20 \mu\text{S cm}^{-1}$ – 24 mS cm^{-1}). The relationship between ρ and R is linear ($R^2 = 0.999$), and the intercept of this plot ($\rho = 0$, $R = 168 \pm 15 \Omega$) represents a constant, additional system R , which is high due to the use of BDD as the electrode material. BDD has a higher resistivity compared to metal electrodes.²⁵ To obtain R_{sol} , this resistance is subtracted from the measured R values so that solution conductance ($G = 1/R_{\text{sol}}$) against solution σ can be plotted (Figure 4b), the gradient of which is equal to $1/\kappa = 0.176 \pm 0.002 \text{ cm}$. A linear response for G versus σ with a very similar gradient ($0.174 \pm 0.003 \text{ cm}$) was also observed in KNO_3 ($\sigma = 16 \mu\text{S cm}^{-1}$ – 23.6 mS cm^{-1} , SI3). The upper end of the linear working range was found to be at $\sigma \sim 25 \text{ mS cm}^{-1}$, with the measured G reaching a plateau when σ reached 30 mS cm^{-1} ($\sim 0.3 \text{ M KCl}$). This was found to be dependent on f_{samp} (SI4), with the potentiostat used having a limit of 100 kHz. This is sufficient for measuring σ of many different water systems as well as typical supporting electrolyte concentrations commonly used in electroanalytical measurements.

To test the capability of the system to measure the σ of different water samples using SWV, several samples from lakes, rivers, and estuaries around the UK, in addition to tap water from two different laboratories in the University of Warwick, were measured using a commercial conductivity meter and compared to the conductivity extracted from SWV (Table 1), using the SWV parameters outlined in Table 1. The σ of the real world water samples extracted from SWV measurements was within 2.5% of that measured by a commercial conductivity meter, therefore proving that this approach can be used to extract the σ from solutions of an unknown composition.

Non-faradaic and Faradaic Analysis in a Single SWV.

By measuring the SWV i – t response in the non-faradaic potential region, we present three examples of how electro-

Table 1. Conductivity of Real World Water Samples, Collected from around the UK, Measured Both with a Commercial Conductivity Meter and from SWV Analysis

sample	conductivity meter (mS cm ⁻¹)	SWV $n = 246$ (mS cm ⁻¹)	percentage error (%)
tap water (lab 1)	0.503 ± 0.001	0.509 ± 0.03	1.2
tap water (lab 2)	0.571 ± 0.001	0.585 ± 0.04	2.5
Bassenthwaite lake	0.0604 ± 0.0001	0.0592 ± 0.004	2.0
Kenilworth river	0.646 ± 0.001	0.653 ± 0.04	1.1
Hayle estuary	0.430 ± 0.001	0.430 ± 0.02	0.0

chemical understanding of the reaction measurement or system can be enhanced. The first example is in the absence of faradaic reactions, the second and third are in the presence.

In Situ Monitoring of Electrode Fouling in the Absence of Faradaic Electron Transfer. Electrode fouling is always a concern when the electrode is directly in contact with the measurement solution. For example, in complex biological media, adsorption of proteins onto the electrode surface can hinder ET, reducing the rate constant and resulting in reduced analytical signals, decreased limits of detection, and uncertainties on the measurement.⁴⁰ EIS has been used to provide information on electrode fouling by measuring changes in the charge transfer resistance^{18,41} or in some cases, C .^{18,20} Here, we investigate whether C values extracted from SWV in the non-faradaic potential window can be used to infer on electrode biofouling, and we use electrolyte solutions containing mucin to this affect.

Mucin is a group of large glycoproteins consisting of a thread-like peptide backbone with segments containing densely packed carbohydrate side chains, which form a mucosal gel blanket on biological surfaces for protection and lubrication.⁴² Mucins are known to result in electrode fouling.⁴³ Figure 5

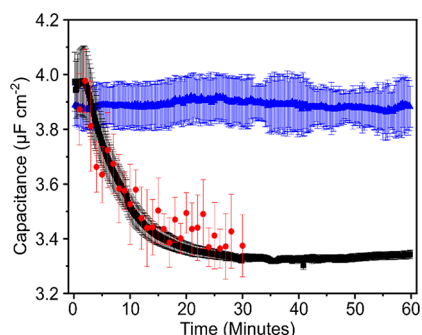


Figure 5. C values in 0.5% w/v mucin and 5 mM KCl measured using SWV (black squares, error bars are the standard deviation in the C values for each scan, $\sigma = 0.707$ mS cm⁻¹) and EIS (red circles). Blue triangles are a control experiment in the absence of mucin at the same σ (0.710 μ S cm⁻¹) measured using SWV.

shows C values, equating to the double layer capacitance, obtained from the SWV response (black squares) for the BDD electrode in a solution of 0.5% w/v mucin in 5 mM KCl. Also shown is C data from SWV measurements (blue triangles) recorded in mucin-free solution (using the same SWV parameters) and EIS data (red circles, error bars are the uncertainty on the fit) at 0.1 V vs SCE, recorded every minute over a time period of 60 min and fitted with an RC equivalent circuit. Due to the increased measurement time, the fastest frequency of measurement for EIS is one measurement per

minute. In contrast, the SWV measurements (black squares, $n = 246$) were performed every 10 s, with each measurement taking only 0.8 s over the potential range of 0.3 to -0.2 V vs SCE ($E_{\text{SW}} = 0.1$ V, $E_1 = 4$ mV, $f_{\text{SW}} = 156$ Hz, and $f_{\text{amp}} = 1$ kHz).

As shown in Figure 5, upon exposure to mucin, C increased slightly and then decreased from a maximum value of 4.03–3.37 μ F cm⁻² over a 30 min time period until reaching a plateau. An increase in R over a comparable time scale was also observed (SIS). The initial starting value for C was as expected based on the data vide supra in the absence of mucin and is close to the control experiment (no mucin), in which C did not decrease with time. A very similar decay was observed in mucin using EIS, fitted with an RC equivalent circuit. In both cases, data fitting is required. For the case of EIS an equivalent circuit must be proposed and the uncertainty on the measurement is determined by the uncertainty on the equivalent circuit fitting. With SWV, the uncertainty can be derived from the standard deviation of repeat measurements. The small but quantifiable decrease in C is attributed to electrode fouling by mucin. Given the BDD surface is oxygen terminated (O-BDD) and thus hydrophilic,²⁵ it is likely that the mucin interacts with the electrode surface through the hydrophilic carbohydrate side chains,^{44,45} rather than hydrophobic bare backbone.

In Situ Monitoring of Electrode Fouling in The Presence Of Faradaic Electron Transfer. Given the results in Figure 5, it is pertinent to verify that fouling information from SWV can also be extracted in the presence of a faradaic reaction. Electrochemical fouling can also occur as a result of electrochemical oxidation (or reduction) of the analyte of interest, due to product adsorption. For example, the oxidation of serotonin, a neurotransmitter, results in the formation of an electrically insulating but porous film due to the formation of a polymer-like film,⁴⁶ formed from reactive side products and dimers.^{47,48} SWV is often used in serotonin detection in order to enhance the electrochemical signature due to the small concentrations detected in typical measurement systems.^{49–51}

To test whether changes in C and R could be recorded using SWV recorded in both non-faradaic and faradaic potential scan regions, repeated SWV scans for the oxidation of 1 mM serotonin in 5 mM KCl over the potential range of 0.45–0.96 V vs SCE were performed (Figure 6a, $E_{\text{SW}} = 0.1$ V, $E_1 = 4$ mV, and $f_{\text{SW}} = 156$ Hz). Non-faradaic SWV information was collected at the foot (shaded green in the inset to Figure 6a) of the SWV faradaic wave (Figure 6a), where no ET is taking place. Analysis of the RC decay curves in the non-faradaic region was conducted using the first 15 reverse pulses ($E = 0.35$ to 0.410 V vs SCE, Figure 6a, inset). From these pulses, extraction of C with repeat scans is also possible (Figure 6c).

As shown in Figures 6a,b, the peak SWV faradaic current drops with repeat scans, attributed to the formation of this porous insulating layer on the surface,⁴⁶ reducing the flux to the electrode surface. The C (Figure 6c) decays similarly, showing a drop with the first scans, followed by a slower decrease, in line with the peak current data (Figure 6b). The decrease in peak current could be due to a variety of effects, including a decrease in electrode area, a decrease in available adsorption sites for serotonin, possible partitioning of serotonin in the polymer film, etc.⁴⁶ This data provides an additional way to measure electrode fouling and allows for in situ real time monitoring of the electrode condition. It can also help distinguish whether the decrease in peak current is due to a change in the serotonin concentration or electrode fouling.

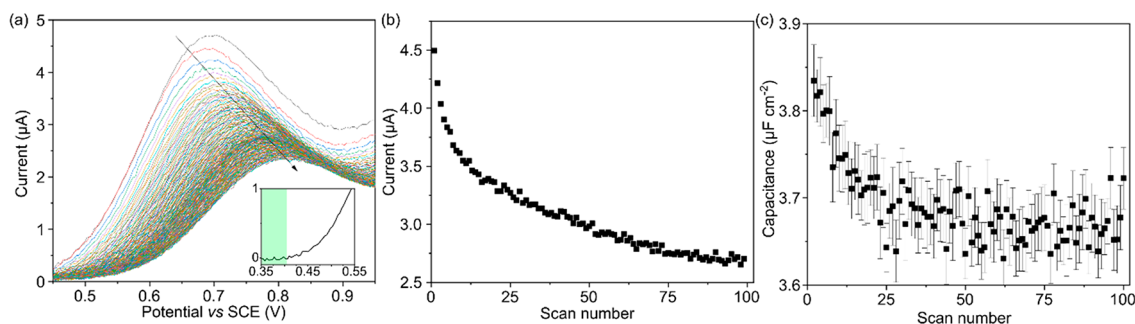


Figure 6. (a) The 100 SWV scans for 1 mM serotonin in 5 mM KCl showing a decrease in the peak current. (Inset) The reverse currents for the first SWV scan, showing a region free from faradaic currents (green, highlighted). The axes are the same as in (a). (b) Change in the SWV faradaic peak current with repeat scans. (c) Fitted C values from the initial (non-faradaic) portion of the SWV, showing a decrease in C upon electrode fouling with repeated scans.

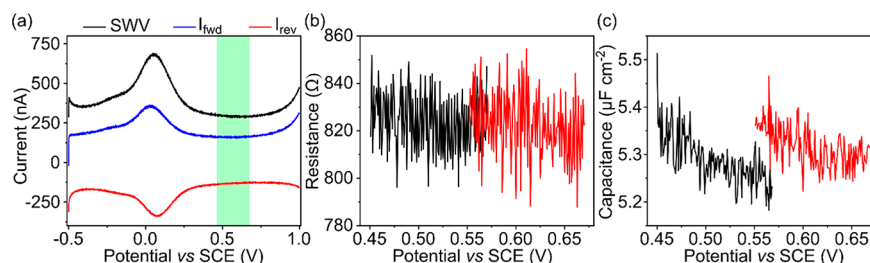


Figure 7. (a) SWV of a laser micromachined BDD electrode in pH 7.09 Carmody buffer ($\sigma = 8.80 \text{ mS cm}^{-1}$, $E_{\text{SW}} = 0.05 \text{ V}$, $E_1 = 1 \text{ mV}$, and $f_{\text{SWV}} = 156 \text{ Hz}$) with a region free of faradaic reactions highlighted (green). Fitted R (b) and C (c) values from the non-faradaic region of the SWV ($E_{\text{SW}} = 0.05 \text{ V}$, $E_1 = 1 \text{ mV}$, and $f_{\text{SWV}} = 1.67 \text{ kHz}$).

Use of One Electrode To Determine Both pH and Solution Conductivity Using SWV. Previous work has shown that laser ablation of the BDD surface creates quinone groups under proton-coupled electron transfer.^{28,29} In this way, the sp^2 -BDD electrode is now voltammetrically pH sensitive. SWV is used to enhance the pH voltammetric detection signal.^{28,29} Often, for water quality assessment, knowledge of pH and solution conductivity is very helpful. SWV for this electrode in pH 7.09 Carmody buffer ($\sigma = 8.80 \text{ mS cm}^{-1}$, measured using a commercial meter), using the parameters $E_{\text{SW}} = 0.05 \text{ V}$, $E_1 = 1 \text{ mV}$, and $f_{\text{SWV}} = 156 \text{ Hz}$, shows a pH sensitive faradaic peak (Figure 7a), where the black line is the output SWV response (current sampled at 75–100% of the pulse). The blue and red lines show the forward and reverse currents. Also, a potential window is clear, 0.45 to 0.67 V vs SCE, where no faradaic reactions occur (Figure 7a, green region). SWV data were recorded in this window using the same parameters as for pH, except the frequency was increased to 1.67 kHz to capture the non-faradaic contribution in this high conductivity region. Note, the need to increase f is purely a limitation of our measurement system in terms of the number of data points available. In this region, R and C could be measured from the raw $i-t$ of an SWV (Figure 7b,c, respectively).

The average value for R ($820 \pm 14 \text{ } \Omega$, $n = 246$) could be used to calculate the solution conductivity $= 8.73 \pm 0.19 \text{ mS cm}^{-1}$, which is in close agreement with the value measured using an independent commercial conductivity meter. The average C ($n = 246$) was $5.30 \pm 0.05 \text{ } \mu\text{F cm}^{-2}$, higher than the unmachined electrodes used *vide supra*, as would be expected for a BDD electrode with an sp^2 surface component.⁵²

CONCLUSIONS

SWV use, in the majority of cases, focuses only on analyzing current signals in the faradaic window, even though data are recorded in both the non-faradaic and faradaic potential regions of the scan. In this article, we show that by capturing the entire $i-t$ trace associated with the SWV potential pulse sequence and analyzing the data in the non-faradaic region of the potential window, additional information can be obtained on the measurement system of interest. We highlight three particular areas. All take advantage of the fact that, in the non-faradaic region, the $i-t$ decays per potential pulse can be directly linked to the solution resistance (and solution hence conductivity) and the double layer capacitance of the electrode.

In particular, (1) knowledge of how the $i-t$ decays in the non-faradaic region can be used to optimize SWV parameters, such that, in the faradaic region, the current SWV output is entirely free from non-faradaic contributions. (2) The SWV capacitance data can be used to provide real time monitoring on whether a changing faradaic signal is due to concentration changes of the electrochemically active analyte or fouling of the electrode. (3) The SWV resistance measurement can be used to inform on the conductivity of the solution, negating the need for an additional conductivity probe to be added to the solution. Finally, if the faradaic current decay profiles are well understood, we postulate that subtraction of this data from the initial part of a faradaic plus non-faradaic $i-t$ decay profile could allow for extraction of non-faradaic currents, even when faradaic processes are present.

■ ASSOCIATED CONTENT

■ Supporting Information

The Supporting Information is available free of charge on the ACS Publications website at DOI: 10.1021/acs.analchem.9b01857.

Collecting complete current–time data from an SWV measurement, effect of solution conductivity on measured electrode double layer capacitance, effect of solution conductivity on measured conductance in KNO₃, effect of sampling frequency on measured conductance, and change in measured resistance upon mucin fouling (PDF)

■ AUTHOR INFORMATION

Corresponding Author

*E-mail: j.macpherson@warwick.ac.uk.

ORCID

Samuel J. Cobb: 0000-0001-5015-8090

Julie V. Macpherson: 0000-0002-4249-8383

Notes

The authors declare no competing financial interest.

■ ACKNOWLEDGMENTS

We acknowledge the Royal Society for an Industry Fellowship for J.V.M. (INF/R1/180026) and the Centre for Doctoral Training in Diamond Science and Technology (EP/L015315/1) with the Defence Science and Technology Laboratory (Dstl) for S.J.C. We thank Element Six Ltd. for producing the all-diamond BDD electrode; the Centre for Ecology and Hydrology, Lancaster, UK, for the collection of Bassenthwaite lake water samples; and Alexandra J. Borrill (Chemistry, Warwick) for the collection of Kenilworth river water samples.

■ REFERENCES

- (1) Osteryoung, J. G.; Schreiner, M. M. *C R C Crit. Rev. Anal. Chem.* **1988**, *19* (1), S1–S27.
- (2) Barker, G. C.; Gardner, A. W. *Analyst* **1992**, *117*, 1811–1828.
- (3) Mirceski, V.; Komorsky-Lovric, S.; Lovric, M. *Square Wave Voltammetry: Theory and Application*; Springer: Berlin, Heidelberg, 2007.
- (4) Ramaley, L.; Krause, M. S. *Anal. Chem.* **1969**, *41* (11), 1362–1365.
- (5) Krause, M. S., Jr; Ramaley, L. *Anal. Chem.* **1969**, *41* (11), 1365–1369.
- (6) Christie, J. H.; Turner, J. A.; Osteryoung, R. A. *Anal. Chem.* **1977**, *49* (13), 1899–1903.
- (7) Bard, A. J.; Faulkner, L. R. *Electrochemical Methods: Fundamentals and Applications*, 2nd ed.; Wiley: New York, 1980.
- (8) Lovric, M. *Ann. Chim.* **1994**, *84* (7), 379–382.
- (9) Myland, J. C.; Oldham, K. B. *Anal. Chem.* **2000**, *72* (17), 3972–3980.
- (10) Komorsky-Lovric, Š.; Lovric, M. *Electrochim. Acta* **1995**, *40* (11), 1781–1784.
- (11) Lovric, M.; Komorsky-Lovric, Š. *J. Electroanal. Chem. Interfacial Electrochem.* **1988**, *248* (2), 239–253.
- (12) Phares, N.; White, R. J.; Plaxco, K. W. *Anal. Chem.* **2009**, *81* (3), 1095–1100.
- (13) Mirceski, V.; Laborda, E.; Guziejewski, D.; Compton, R. G. *Anal. Chem.* **2013**, *85* (11), 5586–5594.
- (14) Mirceski, V.; Lovric, M. *Electroanalysis* **1997**, *9* (16), 1283–1287.
- (15) Mirceski, V.; Guziejewski, D.; Lisichkov, K. *Electrochim. Acta* **2013**, *114*, 667–673.
- (16) Dauphin-Ducharme, P.; Arroyo-Currás, N.; Kurnik, M.; Ortega, G.; Li, H.; Plaxco, K. W. *Langmuir* **2017**, *33* (18), 4407–4413.
- (17) Gray, J. R. *Environ. Instrum. Anal. Handb.* **2005**, 491–510.
- (18) Moulton, S. E.; Barisci, J. N.; Bath, A.; Stella, R.; Wallace, G. G. *Electrochim. Acta* **2004**, *49* (24), 4223–4230.
- (19) Contu, F.; Elsener, B.; Bohni, H. J. *Biomed. Mater. Res.* **2002**, *62* (3), 412–421.
- (20) Contu, F.; Elsener, B.; Bohni, H. J. *Biomed. Mater. Res., Part A* **2003**, *67A* (1), 246–254.
- (21) Orazem, M. E.; Tribollet, B. *Electrochemical Impedance Spectroscopy*, 2nd ed.; Orazem, M. E., Tribollet, B., Eds.; John Wiley & Sons, 2017.
- (22) Anderson, J. E.; Bond, A. M. *Anal. Chem.* **1983**, *55* (12), 1934–1939.
- (23) Sher, A. A.; Bond, A. M.; Gavaghan, D. J.; Gillow, K.; Duffy, N. W.; Guo, S. X.; Zhang, J. *Electroanalysis* **2005**, *17* (15–16), 1450–1462.
- (24) Kennedy, G. F.; Bond, A. M.; Simonov, A. N. *Curr. Opin. Electrochem.* **2017**, *1* (1), 140–147.
- (25) Macpherson, J. V. *Phys. Chem. Chem. Phys.* **2015**, *17* (5), 2935–2949.
- (26) Carmody, W. R. *J. Chem. Educ.* **1961**, *38* (11), 559.
- (27) Joseph, M. B.; Bitziou, E.; Read, T. L.; Meng, L.; Palmer, N. L.; Mollart, T. P.; Newton, M. E.; Macpherson, J. V. *Anal. Chem.* **2014**, *86* (11), 5238–5244.
- (28) Ayres, Z. J.; Borrill, A. J.; Newland, J. C.; Newton, M. E.; Macpherson, J. V. *Anal. Chem.* **2016**, *88* (1), 974–980.
- (29) Cobb, S. J.; Ayres, Z. J.; Newton, M. E.; Macpherson, J. V. *J. Am. Chem. Soc.* **2019**, *141* (2), 1035–1044.
- (30) Cobb, S. J.; Ayres, Z. J.; Macpherson, J. V. *Annu. Rev. Anal. Chem.* **2018**, *11* (1), 463.
- (31) Cai, Y.; Anderson, A. B.; Angus, J. C.; Kostadinov, L. N. *J. Electrochem. Soc.* **2007**, *154* (2), F36.
- (32) Liu, D. Q.; Chen, C. H.; Perry, D.; West, G.; Cobb, S. J.; Macpherson, J. V.; Unwin, P. R. *ChemElectroChem* **2018**, *5* (20), 3028–3035.
- (33) Garrido, J. A.; Nowy, S.; Härtl, A.; Stutzmann, M. *Langmuir* **2008**, *24* (8), 3897–3904.
- (34) Xu, J.; Granger, M. C.; Chen, Q.; Strojek, J. W.; Lister, T. E.; Swain, G. M. *Anal. Chem.* **1997**, *69* (19), 591A–597A.
- (35) Alehashem, S.; Chambers, F.; Strojek, J. W. J. W.; Swain, G. M.; Ramesham, R. *Anal. Chem.* **1995**, *67* (17), 2812–2821.
- (36) Kondo, T.; Honda, K.; Tryk, D. A.; Fujishima, A. *Electrochim. Acta* **2003**, *48* (19), 2739–2748.
- (37) Brown, M. A.; Goel, A.; Abbas, Z. *Angew. Chem., Int. Ed.* **2016**, *55* (11), 3790–3794.
- (38) Lust, E.; Jänes, A.; Arulepp, M. J. *Electroanal. Chem.* **2004**, *562* (1), 33–42.
- (39) Bitziou, E.; Joseph, M. B.; Read, T. L.; Palmer, N.; Mollart, T.; Newton, M. E.; Macpherson, J. V. *Anal. Chem.* **2014**, *86*, 10834.
- (40) Hanssen, B. L.; Siraj, S.; Wong, D. K. Y. *Rev. Anal. Chem.* **2016**, *35* (1), 1–28.
- (41) Kiran, R.; Scorsone, E.; de Sanoit, J.; Arnault, J.-C. J.-C.; Mailley, P.; Bergonzon, P. J. *Electrochem. Soc.* **2013**, *160* (1), H67–H73.
- (42) Corfield, A. P. *Biochim. Biophys. Acta, Gen. Subj.* **2015**, *1850* (1), 236–252.
- (43) Fagan-Murphy, A.; Watt, F.; Morgan, K. A.; Patel, B. A. J. *Electroanal. Chem.* **2012**, *684*, 1–5.
- (44) Shi, L.; Ardehali, R.; Caldwell, K. D.; Valint, P. *Colloids Surf., B* **2000**, *17* (4), 229–239.
- (45) Baszkin, A. *Clin. Mater.* **1992**, *11* (1–4), 119–123.
- (46) Patel, A. N.; Unwin, P. R.; Macpherson, J. V. *Phys. Chem. Chem. Phys.* **2013**, *15* (41), 18085–18092.
- (47) Jackson, B. P.; Dietz, S. M.; Wightman, R. M. *Anal. Chem.* **1995**, *67* (6), 1115–1120.
- (48) Wrona, M. Z.; Dryhurst, G. *Biochem. Pharmacol.* **1991**, *41* (8), 1145–1162.

- (49) Park, S. G.; Park, J. E.; Cho, E. I.; Hwang, J. H.; Ohsaka, T. *Res. Chem. Intermed.* **2006**, 32 (5), 595–601.
- (50) Goyal, R. N.; Gupta, V. K.; Oyama, M.; Bachheti, N. *Talanta* **2007**, 72 (3), 976–983.
- (51) Tertis, M.; Cernat, A.; Lacatis, D.; Florea, A.; Bogdan, D.; Suciu, M.; Săndulescu, R.; Cristea, C. *Electrochem. Commun.* **2017**, 75, 43–47.
- (52) Ayres, Z. J.; Cobb, S. J.; Newton, M. E.; Macpherson, J. V. *Electrochem. Commun.* **2016**, 72, 59–63.